Design of sustainable porous materials based on 3D-structured silica exoskeletons, *Diatomite*: Chemico-physical and functional properties

B. Galzerano [a,b], I. Capasso [a], L. Verdolotti [b,*], M. Lavorgna [b], P. Vollaro [c], D. Caputo [a], S. Iannace [b], B. Liguori [a,b]

[a] *Applied Chemistry Labs-Department of Chemical, Materials and Industrial Engineering, University of Naples Federico II, Naples, Italy*
[b] *Institute for Polymers, Composite and Biomaterials, National Research Council, Naples, Italy*
[c] *Technological District on Engineering of Polymeric and Composite Materials and Structures, - IMAST, P.zza Giovanni Bovio 22, 80133 Naples, Italy*

HIGHLIGHTS

- Novel diatomite-based foams were designed by using a natural source, diatomite, vegetable surfactant and silicon powder.
- The materials design lead to an hierarchical porosity from macro (until 500 μm) to nano-scale (under 50 nm).
- Hierarchical porosity of the diatomite-based highlight co-existence of acoustic and thermal insulation properties.
- Diatomite has a significant effect on thermal conductivity reduction, around 46% with respect to the pristine foam.
- The wettability results highlighted that the diatomite-based foams could be potentially used as oil/water membrane too.

GRAPHICAL ABSTRACT

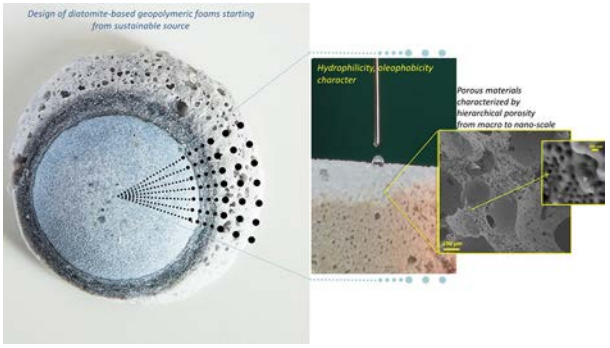

article info

Keywords:
Sustainable chemical-*Diatomite*
Porous material
Silicate solution
Wettability
Thermal-acoustic insulation

abstract

3D-structured silica exoskeletons-diatomite was used as reactive inorganic ingredient, with and without metakaolin to produce sustainable multifunctional diatomite-based geopolymeric foams. Suitable amount of Silicon powder and vegetable surfactant were used as foaming agents, while polysilicate solution was used as reactive crosslinker. The resulting porous materials, characterized by hierarchical porosity ranging from macro to nano-scale, were fabricated at 40 °C for 24 h and characterized by means of chemical and morphological investigations, contact angle, thermal and acoustic properties and fire reaction. The presence of diatomite in the produced foams provides an increase of thermal inertia, and the thermal insulation performance firstly due to the intrinsically low thermal conductivity of diatomite and also because silicon and vegetable surfactant are able to promote the formation of a co-continuous mesoporous structure. Furthermore, the created morphological structure provides a good acoustic absorption coefficient in a wide range of frequency. Finally, due to their hydrophilicity/oleophobicity character, diatomite-based geopolymeric foams could, potentially, be proposed as oil/water separation membranes.

* Corresponding author.
E-mail address: letizia.verdolotti@cnr.it (L. Verdolotti).

1. Introduction

Design and control of hierarchical porosity (micro, *meso* and macroporosity) are the key tasks in the development of new lightweight porous materials with enhanced chemico-physical and functional properties (acoustic and/or thermal) [1,2]. Generally, these materials, based on organic composites, polymers, metals, glass, graphite and cement, are used for thermo-acoustic insulation, cushioning, energy storage as well as catalysis and membranes (as filters) [3–5]. However, the manufacturing processes used to produce them are expensive and consume a significant amount of energy, leading to the emission of huge amounts of carbon dioxide, which is the main cause of the greenhouse effect [6]. In this scenario, it is very important to develop an inexpensive, energy-saving and environmentally friendly acoustic and thermal insulting material to replace existing ones.

For economic and environmental considerations, geo-materials and geo-materials synthesized composite, provide an interesting alternative to the traditional materials, i.e. polymers and cement [7,8]. These materials are obtained by reacting an alumino-silicate powder with a highly concentrated aqueous alkali hydroxide and/or silicate solution, producing a synthetic amorphous-to-semicrystalline alkali alumino-silicate new phase. Furthermore, to improve some mechanical (flexural stress, toughness) and/or functional (acoustic or thermal insulation) performances both fiber reinforcement and porosity can be exploited [9,10]. Different methods may be adopted to obtain porous material, such as application of a limited thermal treatment to a compact pressed powder, formation of foams by dispersing hollow particles in a matrix [11] or using of a pore forming agent [12]. In this case the foaming approaches allow tailoring the cellular structure of the alkali-activated materials in the *meso* to macro range.

Previous study has already shown the possibility of synthesizing geomaterial foam based on metakaolin as matrix and potassium or sodium silicate as crosslinker [8,13].

The simultaneous use of in situ chemical foaming and protein-assisted foaming has been successfully proposed in a previous paper [14] and it can be considered an innovative approach to tailor the mechanical performances as well as the functional properties of inorganic foams. The synergistic effect of two different foaming agents (chemical and physical blowing agent) can lead to porous materials exhibiting porosity ranging from 150 to 700 μm (mediated between open and closed cellular structure) and mechanical properties intermediated between the ceramic and polymeric foams [14].

In order to enhance the functional properties of aforementioned system a reduction of the porosity at nanometric scale (b100 nm) has been explored, for example, by using a filler with intrinsic nano-porosity dimension.

Diatomite represents a filler with this peculiarity, it is a natural sedimentary rock coming from the siliceous fossilized skeleton of diatoms ($SiO_2 \cdot nH_2O$ and crystallized silica). Besides its amorphous silica content, diatomite [15] commonly contains carbonate and clay minerals, quartz and feldspars and are available in large quantities at low cost. As well described by Li et al. [16], due to their three-dimensional (3D) structured silica exoskeletons, known as frustules (porosity ranging from 100 nm to 100 μm), diatomaceous earths have drawn attention from a different of research fields thanks to their chemically inert, extraordinary mechanical properties, huge surface area (high surface/volume ratio), high water absorbing/retention, and especially unique optical properties. The presence of amorphous silica, their fine porous structure, lightness and low thermal conductivity (0.05–0.10 W/mK) allow them to be used as filtering agent, catalyst carrier and heat, cold and sound insulators [17]. Pimraksa and Chindaprasirt [18] reported significant uses of diatomite in construction and insulation materials.

In a previous paper Liguori et al. [19] designed and characterized an innovative geopolymeric foam, based on metakaolin, as matrix, diatomite as reactive filler, sodium silicate as crosslinker and vegetable surfactant as blowing agent. The effect of diatomite as a partial (or total) replacement of metakaolin was evaluated in terms of mechanical, mineralogical and physical properties of the foams.

In the present paper the focus was shifted on the tuning of the functional properties of the diatomite-based geopolymeric foams: the effect of diatomite reactive-ingredient addition, as a partial (or total) replacement of the metakaolin matrix, on porosity at nanoscale, wettability, thermal stability, fire resistance, thermal conductivity and the acoustic properties of the produced foams was assessed.

2. Experimental

2.1. Materials

The Sodium Silicate (SS) ($SiO_2/Na_2O = 3.2$) was provided by Prochin Italia Srl (wt%: SiO_2 27.40; Na_2O 8.15; H_2O 64.45); the metakaolin powder, MK, was provided by NEUVENDIS with the following composition (wt%): Al_2O_3 42%; SiO_2 53%; K_2O 0.77%; Fe_2O_3 1.60%; TiO_2 1.83%; MgO 0.19%; CaO 0.17%. (Metakaolin is an alumina-silicate powder produced by the thermal decomposition of kaolin, a naturally occurring clay basically containing kaolinite $[Al_2Si_2O_5(OH)_4]$. It is almost completely amorphous with traces of quartz, kaolinite and other clay minerals [19]. The particle size distribution reported in the technical sheet showed the following median diameters: $D_{50} = 3$ μm and a $D_{90} = 10$ μm).

Si metal powder (chemical blowing agent) and Na_2SiF_6 (catalyst) were supplied by Merck and Sigma-Aldrich respectively. Vegetable surfactant (physical blowing agent) in water solution (pH = 7) was supplied by Isoltech s.r.l. Italia and used as received after mechanical whipping. Diatomite, Celite® 545 a calcined diatomite, was provided by Celite France and it has been used as received. The chemical composition is the following (wt%): SiO_2 91.5; Al_2O_3 1.0; Fe_2O_3 1.5; P_2O_5 0.004; CaO 0.3; MgO 0.3; $Na_2O + K_2O$ 2.5 and it could contain up to 70% of crystalline silica as cristobalite (mineralogical crystalline silica phase) [19,20]. The particle size distribution is characterized by a retained on 106 and 45 μm mesh of 25 and 62 (wt%) respectively, with a median particle size of 53.1 μm. (Additional information in terms of morphological structure, SEM images, were reported in Supplementary information, Fig. S1).

2.2. Preparation of diatomite-based geopolymeric foams

A diatomite-based geopolymeric foam (HCF) [19], as control sample, based on: 70 wt% of SS, 8.65 wt% of Na_2SiF_6, 21.3 wt% of aluminosilicate source (MK) and 0.05 wt% of Si powder was prepared. Based on 100 parts of the above mixture 12 part of a "meringue" type foam was added. In particular, the "meringue" was prepared by whipping the vegetable surfactant using an UltraTurrax disperser at 12000 rpm up to obtain a volume 8 times the initial one.

The slurry, HCF, was cast in plastic prismatic open molds (4 × 4 × 16 cm^3) and cured unsealed at 40 °C for 24 h at room humidity. The other foams were prepared by replacing metakaolin (MK) in the starting mixture with different percentage of diatomite from 5 to 100 wt% (namely D-HCF/5, D-HCF/10, D-HCF/50, D-HCF/70, D-HCF/100, where the number represent the percentage of Diatomite).

3. Characterization of diatomite-based Geopolymeric foams

3.1. Porosity and specific surface

In order to characterize porosity and specific surface of the foams, nitrogen adsorption analysis have been performed using a Nova 1000 machine (Quantachrome, USA). Density functional theory (DFT) methods was used for determining pore size distribution in the range from micropore to mesopore [21].

The morphological structure of the diatomite-based geopolymeric foams was assessed by Scanning Electron Microscopy, SEM, (SEM, LEO

1530, Zeiss). The foam samples were cross-sectioned, sputtered, and then analyzed at an accelerating voltage of 20 kV.

3.2. Chemical and physical characterizations

The chemical structure, that can occur during the synthesis of diatomite-based geopolymeric foams, is measured from the band frequency of the transverse-optical (TO_x: TO_1, TO_2, TO_3, TO_4), longitudinal-optical (LO_x: LO_1, LO_2, LO_3, LO_4) and longitudinal-optic-transverse-optical (LO_x-TO_x: LO_1-TO_1, LO_2-TO_2, LO_3-TO_3, LO_4-TO_4) stretching modes of the Si-O-Si bond [22] by means of Reflectance Attenuate Mode (ATR) FT-IR spectroscopy. FT-IR spectra of the samples are collected at room temperature by using a Nicolet apparatus (Thermo Scientific, Italy) from 4000 to 600 cm^{-1} with a wavenumber resolution of 4 cm^{-1} for 64 scans.

The spectral region ranging from 1400 to 600 cm^{-1} was analyzed by deconvoluting the severals peaks with OriginPro 8.0 software. The positions of the absorption bands, corresponding to specific vibrational mode assignments of *TO* (for instance TO_2, that is related to the symmetric stretching of υ_s Si\O and TO_3, that is related to the asymmetric stretching of υ_{as} Si\O), *LO* (for instance LO_2, that is related to the symmetric stretching of υ_s Si\O and LO_3, that is related to the asymmetric stretching of υ_{as} Si\O), and longitudinal-optic-transverse (LO)-TO splitting of vibrational modes (i.e.: LO_4-TO_4) attributed to the disordered-induced modes [19,22] were determined by automatic peak finding feature, by using Lorentzian function for deconvolution.

The wettability on the diatomite-based geopolymeric foams was also evaluated by means of contact angle measurement with goniometer OCA 20 (DataPhysics Instruments, Filderstadt, Germany) at room temperature. This device is based upon a conventional goniometer contact angle apparatus, with the addition of automated drop delivery, digital image capture, and data analysis. Calculations based on measured contact angle values allow to evaluate the wetting characteristics of a solid material [23].

The sample was positioned directly under the dosing needle of a glass microsyringe (DS 500/GT gas tight 500 μL syringe) on the stage of the instrument. Two typologies of liquid analyzers were used: water and diiodomethane. For both a liquids droplet (1 μL) was poured on the surface of the sample and the contact angle was measured by the Software SCA20. Ten measurements for each sample were performed.

3.3. Thermal properties and fire resistance behavior

The thermal degradation of the diatomite-based geopolymeric foams was investigated by thermogravimetric (TGA) and derivative TGA (dTGA) analyses with a TGA 2950 apparatus (T.A. Instruments, USA) under air atmosphere. The samples were heated on platinum pans from 30 to 1000 °C with heating rate of 20 °C/min.

Moreover, in order to evaluate the behavior of the diatomite-based geopolymeric foams in isothermal condition, each specimen was thermally treated at 200, 400 and 600 °C, using a Nabertherm HTC 03/15 oven. The thermal used consisted in a heating ramp with heating rate of 10 °C/min followed by an isothermal step at the fixed temperature for 2 h. Before and after every thermal treatment, the foams were accurately weighted, using a Mettler Toledo XS105 Dual Range microbalance with an accuracy of ±0.1 mg, where the dimensional modifications were measured by using a caliper (accuracy ±0.05 mm).

The thermal conductivity of each foam was measured according to ASTM WK50791-WK43689 at ambient conditions, using the Modified Transient Plane Source (MTPS) technique on a C-Therm TCi Thermal Conductivity Analyzer. The samples were put on a 17 mm diameter sensor. For each system, five tests were performed [24,25].

The fire behavior, exhibited by diatomite-based geopolymeric foams in realistic fire conditions, was evaluated by a cone calorimeter and a non-combustibility apparatus. Regarding cone calorimeter tests, an oxygen consumption cone calorimeter (Fire Testing Technology, FFT dual cone calorimeter model) was used. The standard procedure ISO 5660 used in this analysis involves tiles shape specimens (100 × 100 × 20 mm^3) in horizontal orientation subjected to an external radiant flux of 50 kW/m^2, representing a developed fire. Three samples for each system were investigated.

The standard procedure ISO 1182 for non-combustibility tests involves cylindrical specimens (d = 45 mm and h = 50 mm) inserted in a furnace set to 750 °C for 30 min. The parameters measured during test are: the mass lost by the sample in %, total duration (s) of sustained flame (if occurs) and the temperature rise (°C) of the surface and center of the sample and of the furnace during the test.

3.4. Acoustic properties

Thanks to the presence of a partially open-cells (micro- and nano-scale) structure, that permits to the air particles to move through the pores of the material, the sound absorption coefficient (α), was also measured according to the standard UNI EN 10534. For this measurement an impedance Kundt tube, 100 mm in diameter, 570 mm in length was used. The distance between first microphone and samples was 200 mm, while the distance between first and second microphone was fixed at 50 mm. The frequency ranged from 200 to 2000 Hz. A loudspeaker placed at one end of the tube generated the signal (white noise), while the samples are placed on a rigid surface at the opposite end. The thicknesses of foams were equal to 33 mm.

4. Results and discussion

4.1. Porosity and specific surface

The DFT (density functional theory) pore size distributions of diatomite-based geopolymeric foams evidenced the significant change in the porosity that takes place after the replacement of metakaolin with the diatomite (Fig. 1a).

The D-HCF/50 and D-HCF/100 samples showed a very narrow and high peak between the values of about 5 and 7 nm. It is a confirmation of the presence of nanoporosity that derives from the nanopores originally present in the diatomite. HCF does not present this kind of peak and its pore size distribution is characterized by a quite completely flat curve. This means that in the HCF foam, porosity on nanometric scale is somewhat absent as also observed by SEM characterization at high magnification (see the SEM at high magnification in Fig. 1b). As already reported by Liguori et al. [1,19] and as observed in the SEM at low magnification, the HCF cellular morphology showed a porosimetric distribution ranging from 100 to 500 μm, and the pore size decreases with the increasing of diatomite content. On the contrary, D-HCF/50 and D-HCF/100 presented a well-developed porous structure at nanometric scale ranging from 100 to 400 nm. The diatom frustules present in the diatomite are responsible of the formation of a uniform aerogel-like structure (see SEM image of D-HCF/100), deriving from the reaction of diatomite surface with alkaline silicate solution. In fact, due to the reactivity of the diatomite surface in alkaline condition the "individual" shape of diatom disappears creating a co-continuous structure. Instead, as observed in the SEM micrographs (of D-HCF/50 and D-HCF/100) at low magnification the presence of both, chemical and physical, surfactants has induced a formation of micro and macroporosity (as widely described by Liguori et al. [1,19]), assuring the obtainment of hierarchical structure.

This peculiar morphological structure, as already observed in Liguori et al. [19], affects the mechanical performances of the foams: the compressive strength of D-HCF/100 results about 3 times (σ~1,4 MPa at ρ~400kg/m^3) with respect to the HCF (σ~0,50 MPa at ρ~400kg/m^3).

Due to this aerogel- like structure the BET surface value, increases significantly with diatomite content especially for D-HCF/100 sample (from 1.072 m^2/g to 23.202 m^2/g).

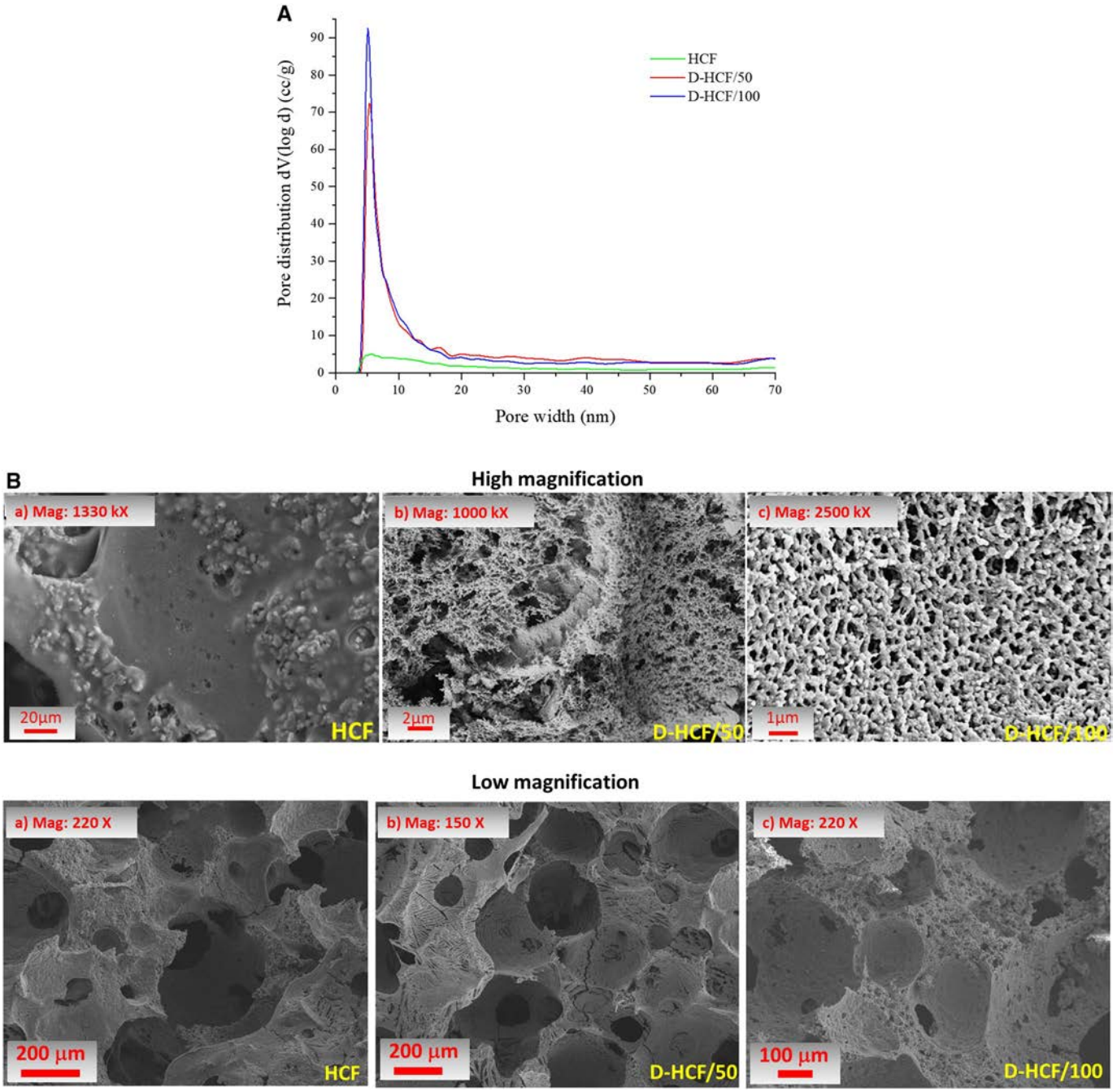

Fig. 1. (a) DFT pore size distributions of HCF, D-HCF/50 and D-HCF/100 samples and corresponding (b) SEM images at high and low magnification.

4.2. Chemical and physical characterizations

Deconvoluted FT-IR spectra related to the different diatomite-based geopolymeric foams are shown in Fig. 2 and the corresponding assignments are listed in Table 1. The absence of stretching vibrations, for all samples, related to the Q^0 and Q^1 units (silica monomer and dimer respectively) suggests a high degree of silicate polymerization, while the stretching vibration of Si-O-2 and 3 non-bonding oxygens, NBO, linkages ($Q^3$and Q^2), characteristic of two or three non-bonding oxygens, are detected in all samples.

The broad absorption band centered around 1030–1140 cm^{-1} is assigned to the overlapping of the vibration modes of the different linkages of silicate structure such as Q^3, TOx and LO_x [19,22,26]. In particular, the contribution of Q^3 decreases by increasing of Diatomite content until it completely disappears for the DHCF/10. Conversely the TO_3 modes as well as the shoulder around 1200 cm^{-1} ascribed to the LO_3 vibrational modes becomes more intense with the diatomite content. As described by Innocenzi [22] the presence of LO_3 vibrational modes show that the structure is highly crosslinked and porous.

However, a shift of TO_3 modes to lower wavenumber was also observed (from D-HCF/5 to D-HCF/100), which could be ascribed to a more porous structure characterized by smaller siloxane rings, larger SiOSi angles and SiO bond lengths. This is due to the degree of condensation reactions of siloxane components which occur between the several ingredients (silicate-silicate, silicate-diatomite surface and silicate-metakaolin). As well described by Innocenzi [22], the condensation reaction during the synthesis of silicate-based foam is accompanied by a shrinkage mono-dimensional perpendicular to the powder surface

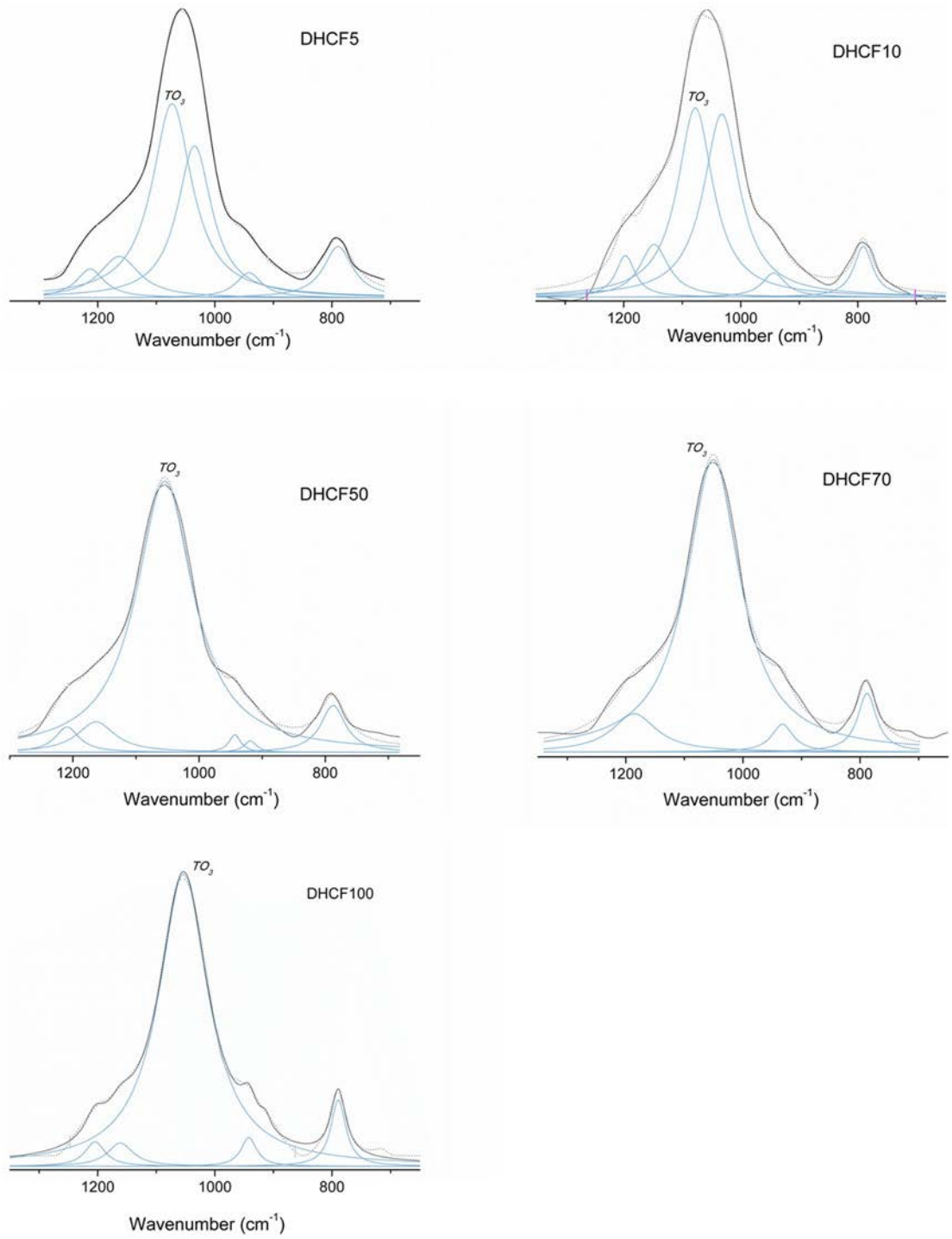

Fig. 2. Deconvoluted FTIR spectra of different diatomite-based geopolymeric foams.

(i.e. diatomite) and, as consequence, a shift in frequency of TO_3 modes could be observed.

The sessile drop experiment is performed on two different surfaces corresponding to the surface exposed to air and to the cut surface (namely external and internal respectively, Fig. S2 in supporting information) of each selected diatomite-based geopolymeric foams. Internal and external surfaces were characterized by different roughness: the first was rougher than the second. The structure of the surface has a direct influence on contact angle and wettability of surface itself: at the macroscopic scale, Wenzel [27] and Cassie-Baxter [28] theories correlate the contact angle behavior to the roughness factor. The Cassie-Baxter model, that is a development of Wenzel's theory, defines the correlation between apparent contact angle on a porous surface with a contribution due to the porosity [29].

In Fig. 3 the images of contact angles related to the droplets of diiodomethane on the internal and external surfaces of different samples are showed. On the external surfaces, the wettability behavior is related to the chemical structure of the foams: in fact, the oleophobic character decreases with the diatomite content. On the contrary, the internal surfaces showed a significant oleophobicity which does not depend on the intrinsic nature of the diatomite-based geopolymeric foams. In fact, a porous material can display a oleophobic character due to the air entrapped within the porous structure, which can prevent the entrance of liquid (diidomethane)

Table 1
FT-IR details of several sample foams.

General assignments [22]	Wavenumber (cm^{-1})
Si-O-Si υ_s (TO_2 and LO_2 modes)	~810–820
Si-O (Q^0)	850–855
Si-O (Q^1)	898–920
Si-O (Q^2)	940–950
Si-O (Q^3)	1030–1040
Si-O (Q^4)	1093–1160
Si-O-Si υ_{as} (TO_3 modes)	1070–1050
Si-O-Si υ_{as} (LO_3 modes)	~1200

Specific assignment [22]	Wavenumber (cm^{-1})				
	D-HCF/5	D-HCF/10	D-HCF/50	D-HCF/70	D-HCF/100
TO_2-LO_2	789	790	787	788	790
Q^1	–	–	–		
Q^2	941	943	944	939	941
Q^3	1034	1032	–	–	–
TO_3	1073	1077	1054	1053	1050
Q^4	1163	1148	1163	–	1161
LO_3	1212	1197	1209	1190	1205

into the pores resulting in higher values of contact angle. Yuqi Teng et al. [30] reported that this behavior could increase with the surface roughness. As expected the contact angle for rougher surface, the internal one, is bigger than the external one. In particular, contact angle increases from 69.3° to 111° for D-HCF/100, from 67° to 91° for D-HCF/50 and from 67° to 96° for HCF.

The wettability radically changes when the liquid is water. In fact, the silico-aluminate nature of all the foam samples leads to a high hydrophilicity. As reported in the Video 1, water droplets were immediately absorbed on all the surfaces, regardless their roughness or nature.

Finally, this wettability behavior showed that the oleophobic character of the proposed foams can be tailored dosing the amount of diatomite. At the same time the foams, due to their composition, exhibit a high hydrophilicity. The above findings suggest a possible application as oil/water separation membranes for remediation of wastewaters containing either organic and/or inorganic pollutants.

4.3. Thermal properties and fire resistance behavior

The thermo-degradative behavior up to 1000 °C was examined for all the foams with TGA/DTGA analysis.

The thermodegradation of ceramic foam showed three decomposition temperatures with maximum values occurring at $T_{maxd1} = 99$ °C, $T_{maxd2} = 554$ °C and $T_{maxd3} = 796$ °C. In Table 2 the degradation temperatures related to each sample are summarized. All the foams show similar weight losses in the same temperature ranges and the total amount weight losses is always near to 10%. In particular, the first range goes from about 50 °C to 200 °C and the weight loss is ascribed to the condensation reactions of the sodium silicate solution [31,32].

The other two main weight losses identified can be both connected to the thermal degradation of the sodium hexafluorosilicate, one of the raw components present in all the different kinds of ceramic foams prepared. In particular, between 550° and 600 °C, there is a very small weight loss (0.45 ÷ 0.65%, see Table 2) that can be attributed to the weight loss of the unreacted sodium hexafluorosilicate. In the temperature range 700°–850 °C, a higher weight loss, equal to about 2%, can be identified and attributed to the vaporization of melted NaF [33], which has been obtained during the consolidation process from the reaction between sodium hexafluorosilicate and sodium silicate solution. The presence of these two phases was already confirmed by XRD analysis, performed on all the diatomite-based geopolymeric foams [19].

In Fig. 4 the weight losses and the volume variations of the samples exposed to thermal cycles are reported. Mass losses increased with temperature for all the foams considered, because the weight loss is due to dehydration processes that are facilitated at higher temperatures. At 600 °C, HCF, D-HCF/50 and D-HCF/100 foams exhibit a very similar value of weight loss (~8–9%). Conversely, at lower temperatures (b600 °C), D-HCF/100 showed a minor weight loss (~5) with respect to HCF and D-HCF/50. Finally, the addition of diatomite leads to an improvement of the final product in terms of volume variation. This trend results to be particularly evident at 600 °C considering that the HCF sample showed a volume reduction of quite 12%, while D-HCF/50 and D-HCF/100 samples showed volume reductions of respectively 5.3% and 3.0%.

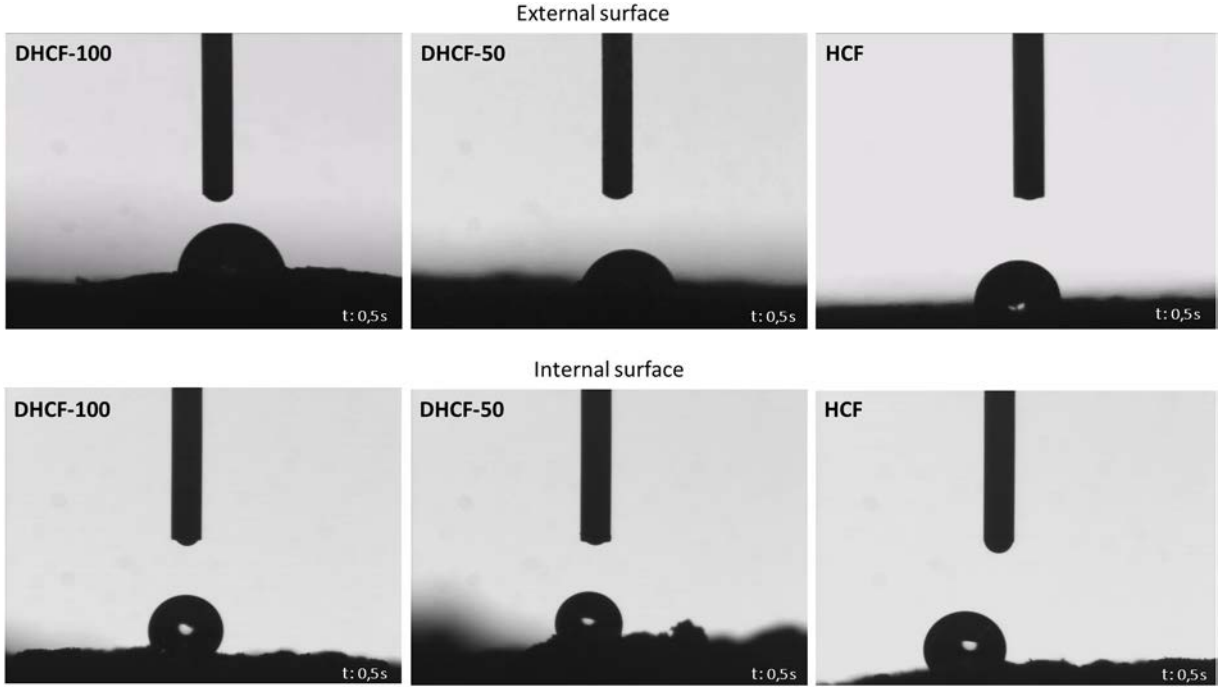

Fig. 3. Contact angle of internal and external surface of HCF, D-HCF/50 and D-HCF/100 with diiodomethane droplets.

Table 2
Main temperature ranges of thermal degradation of ceramic foams.

Sample	T_{max} (°C)	Weight loss-1 (%) (~50°–200°)	T_{max} (°C)	Weight loss-1 (%) (~550°–600°)	T_{max} (°C)	Weight loss-3 (%) (~700°–850°)
HCF	106	4.08	574	0.45	838	2.00
D-HCF/5	96	4.48	560	0.31	840	0.55
D-HCF/10	102	4.52	555	0.60	830	2.06
D-HCF/50	109	4.27	556	0.65	803	2.44
D-HCF/70	103	4.23	555	0.67	810	2.35
D-HCF/100	99	3.56	554	0.50	796	3.88

The positive effect of the diatomite addition on thermal stability of diatomite-based geopolymeric foams is much more significant considering the volume restriction of samples than considering the weight loss. This is probably because all the samples, independently from the diatomite content, contain some unreacted or chemically bonded water that evaporates as consequence of the thermal treatments. On the other hand, the unreacted diatomite, present in the foamed system after the polycondensation [19], acts as filler improving the dimensional stability and hindering the shrinkage of diatomite-based geopolymeric foams.

Thermal conductivity of the diatomite-based geopolymeric foams decreases with increasing diatomite content. Foam HCF shows a thermal conductivity value of 0.128 W/m·K whereas DHCF/50 shows 0.088 W/m·K. The thermal conductivity decreases substantially to 0.074 W/m·K with the total replacement of metakaolin by diatomite. In Fig. 5 the correlation between thermal conductivity, bulk density and diatomite addition is reported. Collected data showed that the thermal conductivity of the foamy materials is not directly correlated to the bulk density. This behavior can be explained by considering that foams showed a nanometric porosity, that influences thermal conductivity through the pores.

In fact, the effective thermal conductivity of a porous material can be described as a combination of different contributions [24,31,34,35]:

$$\lambda_i = \lambda_s + \lambda_g + \lambda_r + \lambda_c \quad [W/m \cdot K]$$

in which:

λ_i is the apparent thermal conductivity of the insulation material; λ_s is related to the conduction through the solid phase (pore walls); λ_g corresponds to the conduction through the gas-filled inside the pores; λ_r is the heat radiation through the cell walls; λ_c is related to the convection within the cells, that is negligible for foams with non-broken

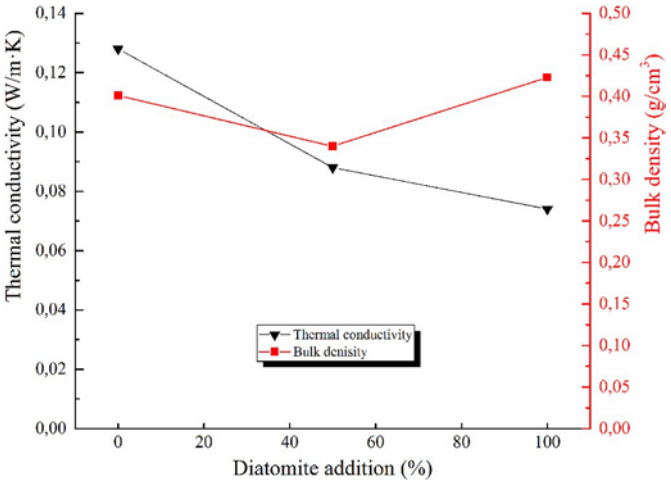

Fig. 5. Correlation between thermal conductivity, bulk density and diatomite addition.

structure, and with cell size smaller than 4 mm, as the Skochdopole experiment confirmed [35].

The solid conductivity λ_S decreases, when thermal resistances increase into the insulating material. Since nano-materials are superior, the solid walls interrupt the heat flow on the nm-level [35,36] and the solid structures (λ_s) influence on the thermal conductivity can be neglected, thanks also to the intrinsically low (0.05 W/m·K) thermal conductivity of the diatomaceous phase. The radiation contribution, λ_r, could account for approximately 30% of the measured effective conductivity at room temperature: it is a non-negligible part of the thermal conductivity of the foam. However, conduction in the cell gas mixture, λ_g, is the main contribution of the thermal conductivity of a foam.

The only way to reduce the overall conductivity is to affect one of the aforementioned contributions. Considering that the cell size of the foams produced is on the range of nanometric, convection is negligible. The "conduction through the gas" contribution, λ_g, can be lowered filling the cells with a gas that has a very low thermal conductivity using a physical expansion [31]. In our case the gas (the air) was not changed. While the presence of nano-pores in diatomite-based geopolymeric foams, especially in DHCF-100, hinder the heat radiation contribution through the cell-walls of the foam, reducing the term λ_r [37].

Cone calorimeter results showed that samples (HCF and D-HCF/50), in the condition of external heat flux selected (50 kW/m^2), do not burn. A very low contribution in terms of heat released rate has been highlighted too (see Fig. S3(a) in supporting information). A little

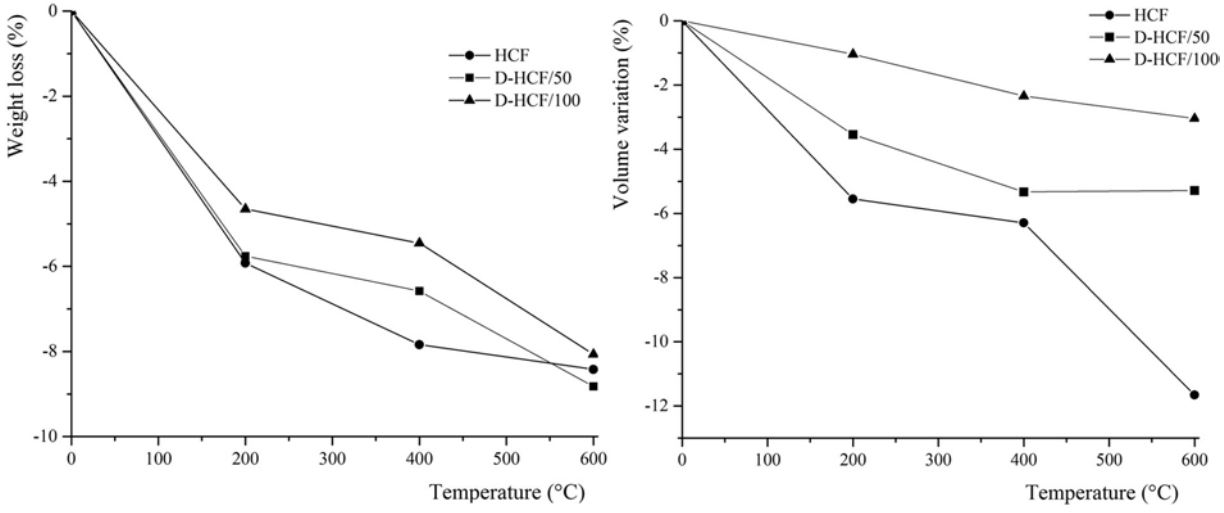

Fig. 4. Weight losses and volume variations of HCF, D-HCF/50 and D-HCF/100 samples after thermal treatments.

Table 3
Non combustibility results related to HCF, D-HCF/50 and D-HCF/100.

Parameters	HCF	D-HCF/50	D-HCF/100
$\Delta T_{(surface)}$ (°C)	1,0 ± 0,4	2,0 ± 0,2	4,0 ± 0,2
$\Delta T_{(center)}$ (°C)	1,1 ± 0,5	1,8 ± 0,3	3,5 ± 0,3
$\Delta T_{(furnace)}$ (°C)	2,1 ± 0,4	1,5 ± 0,1	5,2 ± 0,4
Δwt (%)	10 ± 1	9 ± 1	8 ± 1
Sustained flame (s)	0	0	0

percentage of smoke, which does not reach the concentration necessary to ensure the ignition, is developed (Fig. S3(b) in supporting information), furthermore CO and CO_2 gases are, also, produced in a negligible quantity.

In Table 3 the results of non-combustibility tests in terms of temperature rise of surface and center of sample, temperature rise in furnace, mass lost during the test and development of flame for the three formulations tested have been reported. Samples exhibit a very good fire behavior regardless of content of diatomite; the mass lost during the tests is b15%, flames are not developed, the temperature rise of the surface and center of the sample and in the furnace is less than 10 °C.

The behavior exhibited certifies the non-combustibility of these materials with the best features for application as insulators in the buildings and transport fields (i.e marine). The temperature trend for the non-combustibility test for D-HCF/x samples is reported in Fig. 6.

4.4. Acoustic properties

In Fig. 7 the acoustic absorption curves for selected samples (HCF and D-HCF/50) are reported. Commonly the parameters affecting the acoustic absorption behavior of a porous material are related to the porosity, the tortuosity, the flow resistivity and the thickness of the layer. When the sound propagates in a porous media (with interconnected pores) energy is lost, this behavior is due to the complex heterogeneous microstructure and to the viscous boundary layer effects [38]. In our samples, the results showed a broader "hopscotch" curve with a maximum value of α around 0.47 at 300 Hz for both systems. This behavior is related to the presence of "cavities" that amplify, at specific frequency, the capability to absorb the sound [39]. At higher frequency the two systems, HCF and D-HCF/x, showed two distinct peaks at 1527 and 1248 Hz respectively with a value of α equal to 0.2 and 0.33. The presence of diatomite induced a shift to lower frequency value with an increasing of α value (related to the second peak), probably due to an increasing in tortuosity of porous media. This peculiarity could be enhanced in those applications in which a specific absorption, in a defined range of frequencies, is required.

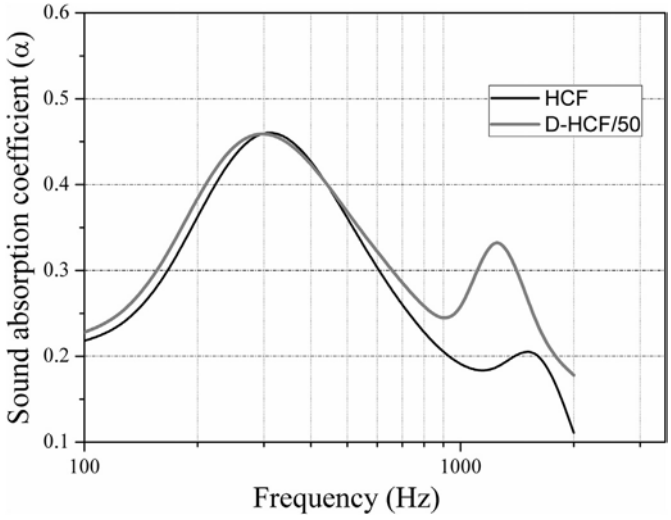

Fig. 7. Sound absorption coefficient as function of frequency for HCF and D-HCF/50 samples.

5. Conclusions

In this paper, the design diatomite-based geopolymeric foams with hierarchical porosity (from macro to nano-scale) were successfully prepared thanks to the synergistic effect of two foaming techniques and diatomite powder as partial (or total) replacement of Metakaolin matrix.

The replacement of Metakaolin with diatomite changes the morphological structure of the produced samples, leading to a porosity on nanometric scale (under 50 nm), preserving also the porosity on a micrometric scale, and to a significant increment in the BET surface value. This morphological structure provided to have at the same time in a unique product either a reduction in thermal conductivity (about 46% for the D-HCF/100 with respect to HCF) and a good capability to absorb the sound thanks to the presence of "cavities" produced by both blowing agents. Furthermore, by increasing the diatomite content (until 100%) an improvement in terms of thermo-dimensional stability (low shrinkage, ~3% at 600 °C for D-HCF/100) and thermal inertia was also observed.

Thanks to the hydrophilicity/oleophobicity character the diatomite-based geopolymeric foams can be also proposed in oil/water separation process for remediation of wastewaters containing either organic and/or inorganic pollutants.

Finally by modulating the formulation it is possible to "design" a foamed products with specific properties ranging from thermal-acoustic insulation to the environment sustainability.

Supplementary data to this article can be found online at https://doi.org/10.1016/j.matdes.2018.02.063.

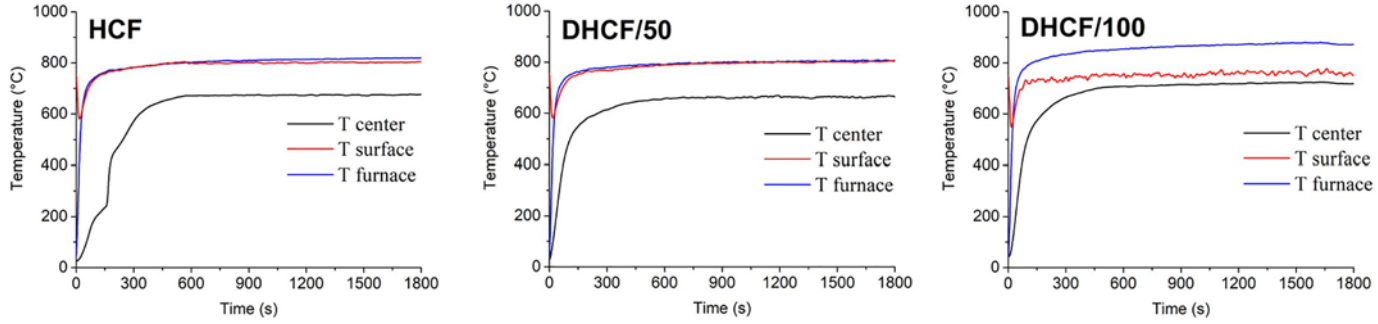

Fig. 6. Temperature trend during the non-combustibility tests for HCF, D-HCF/50 and D-HCF/100.

Data availability

The raw/processed data required to reproduce these findings cannot be shared at this time due to the technical or time limitations.

Acknowledgments

The authors wish to acknowledge all partners of the COCET project ("COmportamento di materiali compositi in Condizioni Estreme: alta Temperatura" - PON02_00029_3206086) and to thank Enza Migliore for graphical and design support of the manuscript.

References

[1] B. Galzerano, L. Verdolotti, I. Capasso, B. Liguori, Setting up the production process of diatomite-based ceramic foams, Mater. Manuf. Process. (2017) 1–6.
[2] R.L. Vekariya, A. Dhar, P.K. Paul, S. Roy, An overview of engineered porous material for energy applications: a mini-review, Ionics 24 (1) (2018) 1–17.
[3] L. Verdolotti, A. Salerno, R. Lamanna, A. Nunziata, S. Iannace, A novel hybrid PU-alumina flexible foam with superior hydrophilicity and adsorption of carcinogenic compounds from tobacco smoke, Microporous Mesoporous Mater. 151 (2012) 79–87.
[4] H. Ren, D. Wu, J. Li, W. Wu, Thermal insulation characteristics of a lightweight, porous nanomaterial in high-temperature environments, Mater. Des. 140 (2018) 376–386.
[5] H.J. Yu, G.C. Yao, X.L. Wang, L.I. Bing, Y.I.N. Yao, L.I.U. Ke, Sound insulation property of Al-Si closed-cell aluminum foam bare board material, Trans. Nonferrous Metals Soc. China 17 (1) (2007) 93–98.
[6] J. Davidovits, Geopolymer cements to minimise carbon-dioxide greenhouse-warming, Ceram. Trans. 37 (1993) 165–182.
[7] P. Duxson, A. Fernández-Jiménez, J.L. Provis, G.C. Lukey, A. Palomo, J.S.J. Van Deventer, Geopolymer technology: the current state of the art, J. Mater. Sci. 42 (2007) 2917–2933.
[8] E. Landi, V. Medri, E. Papa, J. Dedecek, P. Klein, P. Benito, A. Vaccari, Alkali-bonded ceramics with hierarchical tailored porosity, Appl. Clay Sci. 73 (2013) 56–64.
[9] A. Mikhalchan, M. Ridha, T.E. Tay, Carbon nanotube fibres for CFRP-hybrids with enhanced in-plane fracture behaviour, Mat Des 143 (2018) 112–119.
[10] L. Verdolotti, S. Colini, G. Porta, S. Iannace, Effects of the addition of LiCl, $LiClO_4$, and $LiCF_3SO_3$ salts on the chemical structure, density, electrical, and mechanical properties of rigid polyurethane foam composite, Polym. Eng. Sci. 51 (6) (2011) 1137–1144.
[11] D. Zhang, Z. Zhao, B. Wang, S. Li, J. Zhang, Investigation of a new type of composite ceramics for thermal barrier coatings, Mater. Des. 112 (2016) 27–33.
[12] E. Gregorova, W. Pabst, Porosity and pore size control in starch consolidation casting of oxide ceramics-achievements and problems, J. Eur. Ceram. Soc. 27 (2007) 669–672.
[13] M. Scheffler, P. Colombo, Cellular Ceramics: Structure, Manufacturing, Properties and Applications, John Wiley & Sons, 2006.
[14] L. Verdolotti, B. Liguori, I. Capasso, A. Errico, D. Caputo, M. Lavorgna, S. Iannace, Synergistic effect of vegetable protein and silicon addition on geopolymeric foams properties, J. Mater. Sci. 50 (2015) 2459–2466.
[15] L. Davis, Diatomite, ACerS Bulletin, 70(5), 1991, pp. 860–861.
[16] X.W. Sun, Y.X. Zhang, D. Losic, Diatom silica, an emerging biomaterial for energy conversion and storage, J. Mater. Chem. A 5 (19) (2017) 8847–8859.
[17] W. Yuan, P. Yuan, D. Liu, W. Yu, L. Deng, F. Chen, Novel hierarchically porous nanocomposites of diatomite-based ceramic monoliths coated with silicalite-1 nanoparticles for benzene adsorption, Microporous Mesoporous Mater. 206 (2015) 184–193.
[18] K. Pimraksa, P. Chindaprasirt, Lightweight bricks made of diatomaceous earth, lime and gypsum, Ceram. Int. 35 (1) (2009) 471–478.
[19] B. Liguori, I. Capasso, V. Romeo, M. D'Auria, M. Lavorgna, D. Caputo, S. Iannace, L. Verdolotti, Hybrid geopolymeric foams with diatomite addition: Effect on chemico-physical properties, J. Cell. Plast. 53 (5) (2017) 525–536, (0021955X17695092).
[20] N. Ediz, İ. Bentli, İ. Tatar, Improvement in filtration characteristics of diatomite by calcination, Int. J. Miner. Process. 94 (3–4) (2010) 129–134.
[21] J. Landers, G.Y. Gor, A.V. Neimark, Density functional theory methods for characterization of porous materials, Colloids Surf. A Physicochem. Eng. Asp. 437 (2013) 3–32.
[22] P. Innocenzi, Infrared spectroscopy of sol–gel derived silica-based films: a spectra-microstructure overview, J. Non-Cryst. Solids 316 (2) (2003) 309–319.
[23] C. Maldonado-Codina, P.B. Morgan, In vitro water wettability of silicone hydrogel contact lenses determined using the sessile drop and captive bubble techniques, J. Biomed. Mater. Res. A 83 (2) (2007) 496–502.
[24] J. Ma, F. Ye, C. Yang, J. Ding, S. Lin, B. Zhang, Q. Liu, Heat-resistant, strong alumina-modified silica aerogel fabricated by impregnating silicon oxycarbide aerogel with boehmite sol, Mater. Des. 131 (2017) 226–231.
[25] J. Cha, J. Seo, S. Kim, Building materials thermal conductivity measurement and correlation with heat flow meter, laser flash analysis and TCi, J. Therm. Anal. Calorim. 109 (1) (2012) 295–300.
[26] R. Gaggiano, I. De Graeve, J. Mol, K. Verbeken, L. Kestens, H. Terryn, An infrared spectroscopic study of sodium silicate adsorption on porous anodic alumina, Surf. Interface Anal. 45 (7) (2013) 1098–1104.
[27] R.N. Wenzel, Resistance of solid surfaces to wetting by water, Ind. Eng. Chem. 28 (8) (1936) 988–994.
[28] A. Cassie, S. Baxter, Wettability of porous surfaces, Trans. Faraday Soc. 40 (1944) 546–551.
[29] A.K. Kota, J.M. Mabry, A. Tuteja, Superoleophobic surfaces: design criteria and recent studies, Surg. Innov. 1 (2) (2013) 71–83.
[30] Y. Teng, Y. Zhang, L. Heng, X. Meng, Q. Yang, L. Jiang, Conductive polymer porous film with tunable wettability and adhesion, Materials 8 (4) (2015) 1817–1830.
[31] L. Verdolotti, M. Lavorgna, R. Lamanna, E. Di Maio, S. Iannace, Polyurethane-silica hybrid foam by sol–gel approach: chemical and functional properties, Polymer 56 (2015) 20–28.
[32] S. Lirer, A. Flora, A. Evangelista, L. Verdolotti, M. Lavorgna, S. Iannace, Permeation grouting of a fine-grained pyroclastic soil, Ground Improv. 10 (4) (2006) 135–145.
[33] A. Leal-Cruz, M. Pech-Canul, In situ synthesis of Si 3 N 4 in the Na 2 SiF 6–N 2 system via CVD: Kinetics and mechanism of solid-precursor decomposition, Solid State Ionics 177 (39) (2007) 3529–3536.
[34] H.P. Ebert, Aerogels Handbook, 2011 537–563.
[35] R.E. Skochdopole, The thermal conductivity of foamed plastics, Chem. Eng. Prog. 57 (1961) 55–59.
[36] J. Fricke, H. Schwab, U. Heinemann, Vacuum insulation panels–exciting thermal properties and most challenging applications, Int. J. Thermophys. 27 (4) (2006) 1123–1139.
[37] M.G. Kaganer, Thermal insulation in cryogenic, Engineering (1969) 26–49.
[38] M.A. Biot, Generalized theory of acoustic propagation in porous dissipative media, J. Acoust. Soc. America 34 (9A) (1962) 1254–1264.
[39] B.H. Song, J.S. Bolton, A transfer-matrix approach for estimating the characteristic impedance and wave numbers of limp and rigid porous materials, J. Acoust. Soc America 107 (3) (2000) 1131–1152.